

High-Fidelity Radio Communications Modeling for Multi-Robot Simulation

Dylan A. Shell and Maja J. Mataric[‡]

Abstract

This paper describes a high-fidelity model of wireless propagation that integrates several existing models from the wireless communications literature. The model accounts for environmental features, including fading (large and small-scale, and multipath), link-layer models, and interference between radios. In addition to identification and integration of the complementary communication components, this paper's contribution is in demonstrating how discretization, approximation and batch pre-calculation allow the complete model to remain practicable for real-time robot simulation. The faithfulness of the simulated communications is assessed by showing how important qualitative aspects of the communication behavior are reproduced.

1. INTRODUCTION

Recently researchers have become concerned with programming robots to establish and dynamically maintain wireless networks. Such communications may be an end in themselves (e.g., virtual “infrastructure” minimizing goodput, latency, etc.), or the communications may also serve as a means toward some higher-level coordination (e.g., distributed auction algorithms). Even when robots are beyond the range of reliable communication, signal-strength measurements can provide important information. Reproducing realistic network behavior requires modeling both physical and data/application layers, and their interaction.

Although many radio and wireless communication models are available in the literature, no single model adequately captures detailed environmental effects on signal propagation, fading and multipath while simultaneously being fast enough for robotics applications. This paper integrates several models to account for these aspects and achieves suitable runtime performance by relying on a single tedious preprocessing step.

The following section describes existing approaches to simulation of wireless communication and outlines where existing approaches fail to address the needs of roboticists. Section 3 provides a description

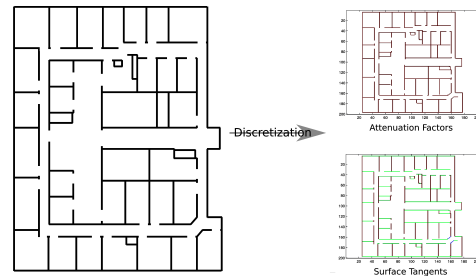


Figure 1. Discretization of the input map.

of the channel model (path attenuation and shape-factor fading) and outlines the division into offline preprocessing and online queries. Section 4 presents examples of variation of signal strength and packet reception rate along a given trajectory. We show conditions with and without interference. These examples at both channel and link-layer levels show good qualitative correspondence with previously identified network behavior.

2. RELATED WORK

This is a high-level analysis of the state of network simulation, first within the robotics and then the sensor-networking communities.

2.1. Robot simulators

Few robotic simulators provide realistic models of wireless network failures or unreliability (cf. Stage [1], Gazebo [2], Teambots [3], Webots [4]¹). The user must perform sophisticated processing to reproduce realistic network behavior, e.g., accessing simulated position information to apply distance-based connectivity rules. This requires additional user code and, consequently, no single approach is pervasive or standardized.

Occasionally researchers use a simple model of network unreliability to show that their control software is robust to communications failures. For example, software might be shown to cope with a complete communications failure, a network partition, or a bounded message loss rate. In such circumstances wireless networks are used purely for communication and, thus, failure

^{*}This work was supported by DARPA under the LANdroids Project

[†]Univ. of Southern California. {shell|mataric}@usc.edu

¹Webots adds white Gaussian noise to IR transmission that, while producing nondeterminism, hardly constitutes a propagation model.

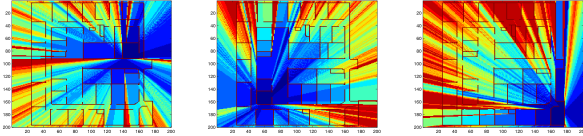


Figure 2. Three examples of path attenuation factors (PAF) from a transmitter placed within the environment. These values are calculated by ray-casting and integrating values along the connecting ray. Partition values for brick from those reported in [8].

models consider only the link-layer behavior. When robots use packet reception and network topologies (or local changes thereof) as important inputs, then these techniques are inadequate.

2.2. Sensor-networking models and simulators

Several standardized models exist within the sensor-network literature. Multiple models exist because they each capture some aspect of network behavior, or have useful theoretical properties, or account for some controlled empirical measurements. Despite several assumptions being shown to be poor approximations of reality, they continue to be used [5]. For example, a popular model considers the communications reception area to be a disc centered on the transmitter. This single radius model is regarded as unrealistic, even for theoretical models [6], but nevertheless its use remains widespread.

Although attempting to study network performance by analyzing performance across layers can be productive in particular applications (e.g., timing analysis in [7]), most models of network performance consider some subset of the layer model. Comparatively little work considers the effects that changing transmission channel conditions have on performance. This is perhaps unsurprising given that sensor networks are typically deployed in fixed locations and that events being monitored are assumed to be sensed through specially designed sensors rather than changes in radio transmission. (There are exceptions to this last case, but the generalization is broadly true.) Thus, modellers will often use a simplified channel model that uses a statistical description of communication channel properties. For example, variance to account for shadowing is often represented by a random variable drawn at initialization time. This suits the sensor network researcher who is not concerned with the spatial relationship of the nodes, but is content with drawing a sample network from an ensemble which describes plausible networks. One finds examples of sophisticated models of application-layer network performance, interference, etc., despite the physical channel properties being simple.

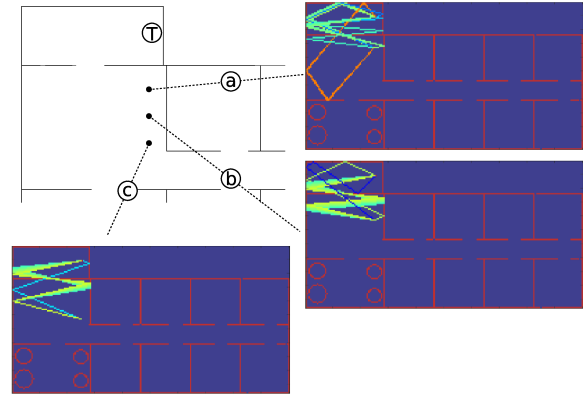


Figure 3. Ray-tracing allows the reflected components of the received power to be calculated. This is used to construct an angular distribution of the power, which is summarized with the three shape-factors (for clarity, the power produced by the direct path is omitted from the figure.) The resulting shape-factor for the shown points are: $\Lambda_a = 0.985525$, $\gamma_a = 0.590345$, $\Theta_a = 0.291113$; $\Lambda_b = 0.662603$, $\gamma_b = 0.843989$, $\Theta_b = 0.046750$; $\Lambda_c = 0.762548$, $\gamma_c = 0.388172$, $\Theta_c = -0.191796$.

Such statistical approaches to channel models (e.g., log-normal shadowing [8]) are inadequate for describing performance in contexts in which a robot uses its radio as a sensor of transmission channel properties. As a robot moves, the communications model must reflect the changes in transmission quality (or received signal strength) that result. Indeed, we expect that the robot could potentially use these changes to infer information about structural changes in the world. With mobile nodes, location-based variation becomes important (to see an robotic application that exploits this fact and mobility, see [9]).

2.3. Physical channel models

Broadly speaking, statistical physical channel models, like those mentioned above, attempt to represent underlying causal factors and uncertainty by treating them as randomly drawn from a suitable statistical distribution. The form of the distribution may reflect particular broad categories of environmental types (e.g., Ricean versus Rayleigh fading).

A second class of models considers scenarios in which the physics of the signal propagation can be analyzed. [8] demonstrates how refraction or reflection can be treated in this manner. Since the environments we consider are complex and have small-scale structure, no single such model will suffice. However, this model of radio reflection is used within the ray-tracing approach

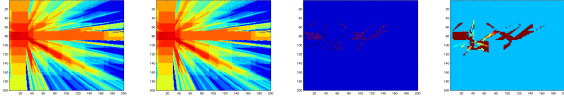


Figure 4. Examples of short-range fading. First (left-most) figure shows the sum of small and large-scale effects. The second and third figures show the large-scale and small-scale components separately. The fourth describes the variance due to small fading; the third figure is sampled from a distribution with this property.

described in the next section.

[8] goes on to describe “site specific” techniques that process a map in order to understand signal propagation within the space. One of these, the primary ray-casting technique, provides a description of large-scale attenuation effects and is used below. Since the map is available to a robotic simulator, it is reasonable to provide the same information to the radio propagation model software. (Additional information like material type, attenuation factor, and surface tangent direction was captured by hand, as shown in the sections the follow.)

Our philosophy is to find potentially computationally expensive techniques that capture the degree to which signal propagation (and hence communication) depends on environmental features. The following section describes more generally the models used. Map pre-processing to enable real-time queries is described thereafter.

3. APPROACH

We are primarily concerned with capturing the effects of position within the environment on reception power. The probability of correct packet reception is a function of the received power. Thus, the channel model must capture the power received from a given transmission location to other areas within the environment. We consider two contributing factors: (1) attenuation as the result of path loss; (2) multipath effects.

3.1. Large-Scale Path Loss

We model the wireless channel by combining a term for large-scale path loss, and a second term for small-scale multipath effects and fading. The log-normal shadowing model is a simple and widely agreed upon model [10], that serves as a reasonable starting point:

$$PL(d) = PL(d_0) + 10n \log_{10}\left(\frac{d}{d_0}\right) + X_\sigma,$$

This gives an value of average power (in dB) lost over the path from a position of length d (where $d \geq d_0$, provided one has some power measurements at d_0). The additional zero-mean normal noise X_σ may change with time, and is used to capture unmodeled effects.

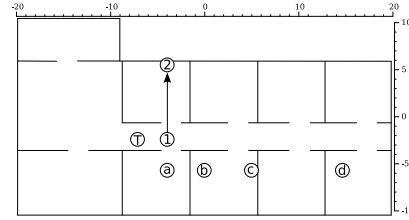


Figure 5. Tests of the model consider a static transmitter T and a receiver that moves from 1 to 2. Interference from radio at a, b, c and d were also considered.

As stated above, our philosophy is to find possibly computationally expensive, but better than resigning ourselves to purely stochastic models. Following [8], Section 4.11.5, we include a terms for shadowing by adding including a path obstructions through so-called “primary ray tracing” so that partition attenuation factor (PAF) values model power loss due passing through an obstacle:

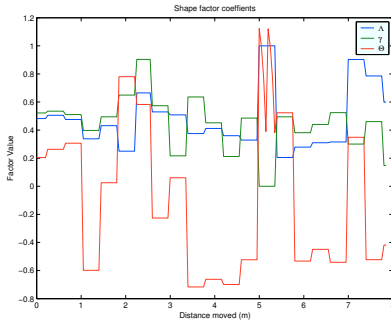
$$PL(d) = PL(d_0) + 10n \log_{10}\left(\frac{d}{d_0}\right) + \sum PAF[dB] + X_{\sigma'}.$$

(Note that variance of the additional noise $X_{\sigma'}$ is decreased because large-scale pass loss is well accounted for by the attenuation factor [8, pp. 163].)

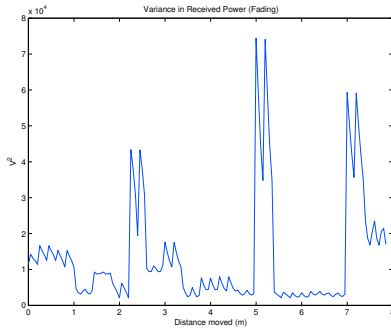
Figure 1 is a plan of a building used throughout the remainder of the paper. Figure 2 graphically shows attenuation factor values for a transmitter in the upper-left corner: these are constructed by ray-casting to sum the attenuation factor values along a path from the transmitter to each part of the environment. (A slight modification like that in [11] handles multi-floored environments easily.)

3.2. Small-Scale Fading

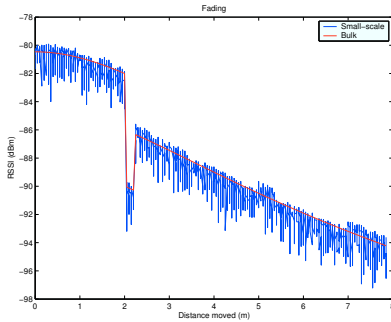
Small-scale fading is produced by two multipath effects: Time-delay spread, and Doppler spread [8, pp. 206]. In our scenarios we consider Flat Fading as the time-delay element, and what is termed slow Doppler Fading. Oftentimes these details will be ignored and either Rayleigh or Ricean distributions used to model the small-scale fading. Rayleigh fading results when there is no line-of-sight between the transmitter and receiver; the receiver is assumed to have power arriving from all angles. Ricean is similar, having power arriving from all angles, but additionally includes power peak to account for a line-of-sight transmission. Much like the use of a normal distribution to model large-scale path loss and shadowing, we were unsatisfied with the lack of an environmental attributes of the behavior in these distributions. We implemented a multipath shape-factor model, which produces Rayleigh and Ricean distributions when arriving power is one of the special cases described above. The following description follows [12].



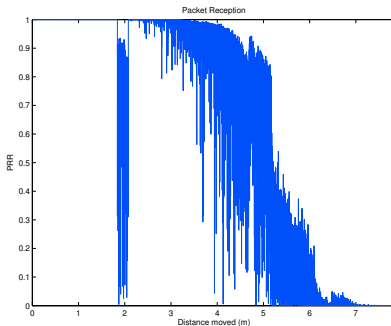
(a) Shape-factors calculated along trajectory.



(b) Variance in received power along trajectory.



(c) Superposition of bulk and small-scale fading effects.



(d) Packet-reception rate along the trajectory.

Figure 6. Radio transmission to a moving test receiver.

The multipath shape-factor model accounts for the fading statistics by modeling the angular distribution of the power, $p(\theta)$ that arrives at a receiver. To calculate this distribution, a deterministic ray tracer was developed that treats obstacles as sources of reflection. Obstacles are modelled as imperfect dielectrics, and assuming an E-field normal to the edge of the obstacle (which holds when E-field is horizontally polarized, and the antenna are placed vertically). If an incident wave entering the obstacle at an angle θ_i has electric field E_i then the reflected wave:

$$E_r = \frac{\sin \theta_i - \sqrt{\epsilon_r - \cos^2 \theta_i}}{\sin \theta_i + \sqrt{\epsilon_r - \cos^2 \theta_i}} E_i.$$

(The relative permittivity ϵ_r is taken as having the value of 4.44 as is suitable for brick.)

The shape-factors are based on the Fourier coefficient's of the power distribution. Once $p(\theta)$ has been calculated for a particular transmitter and receiver pair, we calculate:

$$F_n = \int_0^{2\pi} p(\theta) e^{-in\theta} d\theta.$$

From these the three shape-factors are defined:

Angular spread is a measure of the concentration of power about a single azimuthal direction:

$$\Lambda = \sqrt{1 - \frac{|F_1|^2}{F_0^2}}.$$

Angular constriction is a measure of the concentration of power about a two azimuthal directions:

$$\gamma = \frac{|F_0 F_2 - F_1^2|}{F_0^2 - |F_1|^2}.$$

Azimuthal direction of maximum fading is given by:

$$\Theta = \frac{1}{2} \arg\{F_0 F_2 - F_1^2\}.$$

The variance of the received power (in Volts-squared) is equal to the magnitude-squared of the complex voltage. Figure 3 provides an example. The radio power less the path-loss factor provides P_R (an average of the local received power) and then the variance (from [8], pp. 233) of the complex voltage for a receiver travelling in direction β is:

$$\sigma_{V_r}^2 = \frac{2\pi^2 \Lambda^2 P_R}{\lambda^2} (1 + \gamma \cos(2\beta - 2\Theta)),$$

where λ is the wavelength of the carrier frequency.

Thus, the variance of the received power due to small-scale effects can be calculated from a given transmitted location to a given receiver once the values for Λ , Γ and Θ have been established for that pair. Figure 4 displays the additional variance that results from small-scale effects. The right-most figure shows the variance from the given transmission point. This variance is significant in regions which can be reached from the transmitter through reflection off obstacles.

3.3. Link-Layer Model

Next, we implemented the link-layer model developed by [13], the following is an overview. As mentioned $P_R = P_T - PL_T(d, \Lambda, \gamma, \Theta, \beta)$, where P_T is the radio's transmit power, and $PL_T(\cdot)$ is the sum of $PL(d)$ and the appropriate noise generated as a function of the shape factors just described. The probability of a bit error is modeled by assuming NRZ encoding with NCFSK modulation. This in turn leads to the following expression for the probability of receiving a packet correctly:

$$PRR = \left(1 - \frac{1}{2}e^{-\frac{\alpha}{2}}\right)^{8f},$$

where f is frame length, we take $f = 50$ bytes. The α is the signal-to-noise ratio in [13], but we extend their model as described in the following section.

3.4. Transmission Interference Model

The concurrent transmission model based on [14] is integrated by having signal-to-noise term become a signal-to-interference-plus-noise-ratio. This involves including the power that is received from concurrent transmissions and treating them as adding to the noise floor:

$$\alpha = P_R - P_n - P_I.$$

Both the noise floor P_n and interference are ways that result in asymmetry in the communications network. We follow [13] and generate P_I and P_n together with a covariance matrix that is representative for MICA2 radios. To model P_I , we simulate packet transmission times, and treat a collision on the medium by adding power produced by the interfering transmitter. [14] show that simply adding such noise will overestimate packet losses. Thus, additional interference contributions are halved, based on the data in Figure 13 of [14]. Our experiments suggest packet reception is adversely affected by increasing the interferers more by the increased frequency of collisions than by their contribution to the noise floor.

3.5. Preprocessing and efficient queries

We added this model two multi-robot simulators. The first was our own custom simulator for large swarms of robots, and the second based on Cybele [15].

In order to do this position dependant calculation efficiently, we rely on significant pre-computation. Given transmitter and receiver locations, a model for the power depends on a path attenuation factor (PAF) and three shape-factors coefficients. Two separate databases are produced, one for the PAF values another for the coefficients given any pair of locations within a discretized representation of the environment.

The maps shown in the figures were discretized into a 200×200 grid with each entry storing the attenuation

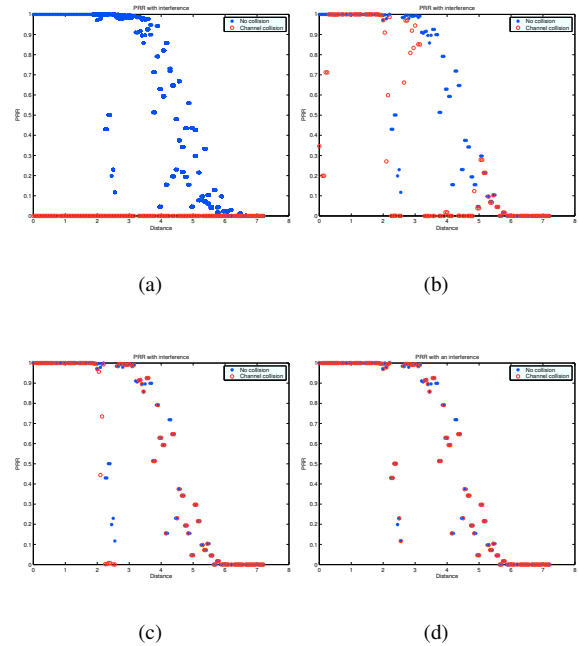


Figure 7. Radio transmission in the presence of interferers, at (a), (b), (c) and (d) respectively.

factor for the material within that portion of the environment, which is then discretized to a 8-bit signed integer. A Path Attenuation Factor Database is produced by ray casting from every possible starting position to every possible final position. The database contains the integral of attenuation factors along a each such trajectory. The process can be optimized by casting long rays initially and storing intermediate values along each ray. We use a Bresenham integer line marching algorithm to perform this quickly.

A Shape Factor Coefficient Database is generated by ray tracing from each position to every other position. This operation takes significantly longer than path attenuation factors, thus we make use of a further down-sampling of the previous grid. Because these operations involve many repeated reflections, an optimization initially builds an index at each surface indexed by a reflection angle.

Both databases are arrays indexed by location 4-tuples. Our implementation memory maps each of these databases in uncompressed form so that, given discretization sizes, the values can be read directly only when needed. This is useful because it does not cause a delay to the simulation start-up.

4. EVALUATION AND DISCUSSION

We briefly present some controlled examples in order to show resulting simulated radio behavior. Figure 5 shows the set-up. A static transmitter at T broadcasts test packets. A test receiver is moved from 1 to 2, which is a distance of about 8 metres. Figure 6 shows the resulting shape-factors, variance in power, total fading, and packet-reception. It is interesting to observe that passing through the doorway from the corridor into the room results in packet reception in the transitional regime of behavior. Notice also how the small-scale effects (see Figure 6(b)) result in marked changes in packet-reception rates shown in Figure 6(d).

This compares favorably with our (and previously published [6, 11, 13]) experience with physical radios in which there exist three basic regimes of behavior: (i) Close, well-connected, near perfect transmission; (ii) Intermediate transitional region with high-variability; (iii) Long distances with no, or very limited connectivity.

The same setup was also used in an arrangement to test interference. The movement of the receiver was repeated, but we included a transmitting interferer at each of (a), (b), (c) and (d) respectively. Figure 7 shows that the effect collisions have on the reception rate varies with position (and hence, received interferer power) as one might expect.

5. SUMMARY

This paper has presents an high-fidelity model of communications for simulation of wirelessly networked robot systems. Our contribution has been in identifying and integrating complementary techniques for capturing the effects of environmental features, fading (large and short-scale, and multipath), link-layer schemes, and interference from other radios. The result is a model that, after a single batch pre-processing stage, can be used to perform rapid, realistic multi-robot simulation. We are unaware of any work that provides these features, which could undoubtedly improve the quality of simulators currently available. We have thus attempted to provide a description of the approach that is sufficiently complete to allow direct implementation.

Acknowledgments

The authors gratefully acknowledge the support provided by DARPA under the LANdroids program.

REFERENCES

- [1] B. P. Gerkey, R. T. Vaughan, and A. Howard, "The Player/Stage Project: Tools for Multi-Robot and Distributed Sensor Systems," in *Proc. Intl. Conf. on Adv. Robotics (ICAR'03)*, pp. 317–323, 2003.
- [2] N. Koenig and A. Howard, "Design and Use Paradigms for Gazebo, An Open-Source Multi-Robot Simulator," in *Proc. IEEE/RSJ Intl. Conf. on Intelligent Robots and Systems (IROS'04)*, pp. 2149–2154, 2004.
- [3] T. R. Balch, *Behavioral Diversity in Learning Robot Teams*. PhD thesis, Georgia Institute of Technology, College of Computing, 1998.
- [4] O. Michel, "Webots: Professional Mobile Robot Simulation," *Intl. J. Adv. Robotic Sys.*, 1(1), pp. 39–42, 2004.
- [5] D. Kotz, C. Newport, and C. Elliott, "The mistaken axioms of wireless-network research," Tech. Rep. TR2003-467, Dartmouth College, Comp. Science, 2003.
- [6] F. Kuhn, R. Wattenhofer, and A. Zollinger, "Ad-Hoc Networks Beyond Unit Disk Graphs," in *Proc. ACM Joint W. on Foundations of Mobile Computing*, 2003.
- [7] M. Maróti, B. Kusy, G. Simon, and Ákos Lédeczi, "The Flooding Time Synchronization Protocol," in *Proc. Intl. Conf. on Embedded Netw. Sensor Sys.*, pp. 39–49, 2004.
- [8] T. S. Rappaport, *Wireless Communications: Principles and Practice*. Prentice-Hall, Inc., second ed., 2001.
- [9] M. Lindhé, K. H. Johansson, and A. Bicchi, "An experimental study of exploiting multipath fading for robot communications," in *Proc. Robotics: Sci. & Sys.*, 2007.
- [10] B. Krishnamachari, *Networking Wireless Sensors*. Cambridge University Press, 2005.
- [11] D. M. Devasirvatham, C. Banerjee, M. J. Krain, and D. A. Rappaport, "Multi-Frequency Radiowave Propagation Measurements in The Portable Radio Environment," *IEEE Conference on Communications*, pp. 1334–1340, 1990.
- [12] G. D. Durgin and T. S. Rappaport, "Theory of multipath shape factors for small-scale fading wirelesschannels," *IEEE Transactions on Antennas and Propagation*, vol. 48, no. 5, pp. 682–693, 2000.
- [13] M. Zuniga and B. Krishnamachari, "Analyzing the transitional region in low power wireless links," in *Proc. IEEE Communications Society Conference on Sensor and Ad Hoc Communications and Networks (SECON'04)*, pp. 517–526, 2004.
- [14] D. Son, B. Krishnamachari, and J. Heidemann, "Analysis of Concurrent Packet Transmissions in Low-Power Wireless Networks," Tech. Rep. ISI-TR-2005-609, USC Information Sciences Institute, 2005.
- [15] Intelligent Automation Incorporated, "Opencybele." <http://www.opencybele.org>, 2009.